JOURNAL OF GUIDANCE, CONTROL, AND DYNAMICS
Vol. 15, No. 4, July–August 1992

On-Line Performance Evaluation of Multiloop Digital Control Systems

Anthony S. Pototzky*
Lockheed Engineering and Sciences Company, Hampton, Virginia 23665
and
Carol Wieseman,† Sherwood Tiffany Hoadley,‡ and Vivek Mukhopadhyay‡
NASA Langley Research Center, Hampton, Virginia 23665

A real-time controller, developed to implement flutter suppression and rolling maneuver load alleviation control laws digitally, was tested on an aeroelastic wind-tunnel model. A controller-performance-evaluation (CPE) methodology to evaluate various multi-input/multi-output digital control systems on line using sampled digital data was also developed and tested. Modern signal processing methods were used to generate appropriate transfer matrices of the control system from the sampled time-domain data of the whole system (controller and plant). Matrix procedures were used to calculate singular values of return-difference matrices at the plant input and output points to evaluate the performance of the control system. The CPE procedures confirmed satisfactory performance of stabilizing control laws and effectively identified potentially destabilizing ones.

Nomenclature

det(•)	= determinant
$\boldsymbol{G}$	= open-loop plant transfer matrix
$\boldsymbol{H}$	= open-loop controller transfer matrix
$\boldsymbol{I}$	= identity matrix
N	= number of time segments
n_a	= number of control-law-output actuator commands
n_s	= number of control-law-input sensor measurements
S_{ux}	= cross-spectrum of excitation to actuator commands
S_{uu}	= autospectrum of excitation, power spectral density
S_{uy}	= cross-spectrum of excitation to plant responses
$\boldsymbol{X}_u$	= controller output transfer matrix
$\boldsymbol{Y}_u$	= plant output transfer matrix
λ	= eigenvalues
σ	= singular values, always non-negative real (A^* is the complex conjugate transpose of A), $\sqrt{\lambda(A^*A)}$
$\overline{\sigma}$	= maximum singular value
$\underline{\sigma}$	= minimum singular value
ω	= frequency

Definitions

stability	= all of the poles of the system are on the left-hand side of the complex plane
robustness	= tolerance of system stability to plant uncertainty that can be measured in terms of minimum singular values or gain and phase margins
performance	= performance of the controller as measured in terms of stability and robustness

Subscripts

A	= additive uncertainty
M_I	= multiplicative uncertainty at plant input point
M_O	= multiplicative uncertainty at plant output point
u	= excitation
x	= controller output
y	= plant output

Sub-Subscripts

c	= signal added at the command location
s	= signal added at the sensor location

Introduction

ACTIVE controls are becoming an increasingly important means to enhance the performance of aircraft. Because the process of designing multi-input/multi-output (MIMO) digital control laws uses relatively untested theoretical methods, it is crucial to evaluate the performance of designed control laws through experimentation. The results of the performance evaluations can then be used to help evaluate the design methods. For classical single-input/single-output (SISO) control systems, analysis tools such as Nyquist diagrams are often used to determine the stability and robustness of the closed-loop system. For MIMO systems, Nyquist techniques are inadequate. Consequently, analytical methods based on the use of singular values of return-difference matrices at various points in the control loop were developed[1–3] to examine the stability and robustness of a control system (SISO or MIMO).

For examining the stability and robustness of digital control systems during testing, the plant is excited by a known input. Experimental time history data consisting of the excitation and system responses (both plant and controller outputs) are acquired. These time history data are then transformed to the frequency domain using fast Fourier transform (FFT) meth-

Presented as Paper 90-3501 at the AIAA Guidance, Navigation, and Control Conference, Portland, OR, Aug. 20–22, 1990; received Nov. 28, 1990; revision received Aug. 23, 1991; accepted for publication Aug. 29, 1991.

*Staff Engineer, NASA Langley Research Center, MS 243, Hampton, VA 23665. Member AIAA.
†Aerospace Engineer, Aeroservoelasticity Branch, MS 243. Member AIAA.
‡Senior Aerospace Engineer, Aeroservoelasticity Branch, MS 243. Associate Fellow AIAA.

ods so that transfer matrices and the return-difference matrices can be computed. Singular values are then determined to obtain measures of system stability and robustness. The steps from acquiring the data through interpreting the singular values comprise a methodology referred to herein as controller performance evaluation (CPE). The methodology is generic in nature and can be used in many types of multiloop digital controller applications, including digital flight control systems, digitally controlled spacecraft structures, and actively controlled wind-tunnel models. These CPE methods were employed during recent actively controlled wind-tunnel testing to check the stability of the closed-loop system to reduce the risk of damage to the wind-tunnel model and the tunnel.

The present paper describes the implementation of the CPE capability, structure of the data flow, signal processing methods used to process the data, and the software developed to generate transfer functions. A brief development of the equations used to obtain the open-loop plant, controller transfer matrices, and return-difference matrices are given. Results of applying the CPE methodology to provide on-line evaluation of digital flutter suppression systems tested on the Rockwell Active Flexible Wing (AFW) wind-tunnel model,[4-6] using the AFW digital controller described in Ref. 7, are presented to demonstrate the CPE capability.

Controller Performance Evaluation

Block diagrams of the basic open- and closed-loop control problems with negative feedback are presented in Fig. 1. The plant to be controlled is represented mathematically by a frequency-domain transfer matrix $\boldsymbol{G}$ with n_s outputs and n_a inputs. The controller is represented mathematically with a transfer matrix $\boldsymbol{H}$ with n_s inputs and n_a outputs. The excitation is used to derive transfer functions between outputs and inputs in either the open- or closed-loop system. The open-loop system is one in which the control law outputs (commands required for controlling plant response) are not fed back into the system as in Fig. 1a, or the sensors are not fed back into the controller as in Fig. 1b. Figures 1a and 1c depict the case when the external excitation u used to excite the system is added at the plant input point. Specifically, in Fig. 1a, the ith plant input is u_{c_i} and the others are zero. In the closed-loop system, Fig. 1c, the ith input is $u_{c_i} - x_i$ whereas the others are $-x_j$. When there are more sensor inputs than control outputs, then the excitation is added at the controller input point as depicted by Figs. 1b and 1d. Specifically, the ith input to the controller is u_{s_i} and the others are zero in the open-loop case. In the closed-loop case, Fig. 1d, the ith controller input is $y_i + u_{s_i}$ whereas the others are y_j. The input to the plant in both cases of Figs. 1c and 1d are the negatives of the controller outputs. When the number of sensors is equal to the number of control outputs, excitations can be applied at either location.

Controller performance evaluation is a two-mode, four-step process. The two modes are open- and closed-loop, and each mode consists of two steps. The process is outlined conceptually for the flutter suppression system application as follows:

Open Loop

Step 1: Verify the controller $\boldsymbol{H}$ by comparing with the designed control law transfer matrix.

Step 2: Predict closed-loop performance based on the open-loop performance to determine whether the control law will stabilize or destabilize the system when the loop is closed.

Closed Loop

Step 1: Determine the stability margins of the closed-loop system during the closed-loop testing by evaluating the singular values of return-difference matrices $(\boldsymbol{I} + \boldsymbol{GH})$, $(\boldsymbol{I} + \boldsymbol{HG})$, and $\boldsymbol{H}(\boldsymbol{I} + \boldsymbol{GH})^{-1}$.

Step 2: Determine open-loop plant stability during the closed-loop testing to determine the open-loop flutter boundary.

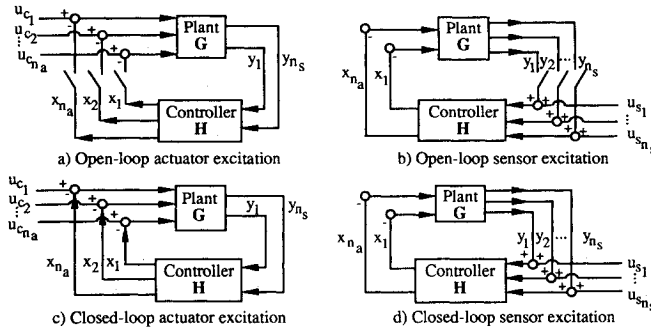

Fig. 1 Controller-plant diagrams depicting the control problem with negative feedback.

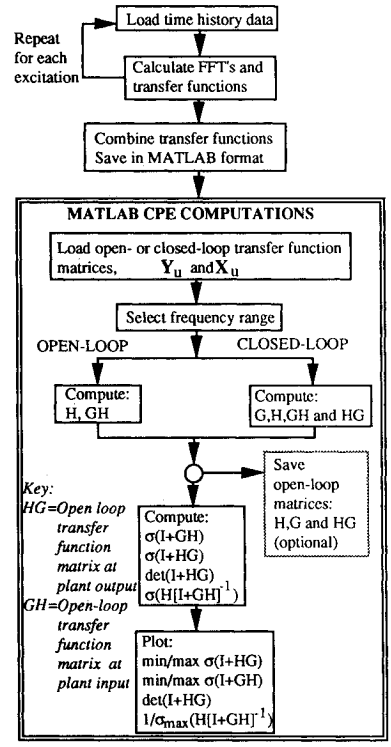

Fig. 2 Flowchart of CPE procedures.

CPE Computations

The CPE computations involve generating frequency-domain transfer functions of plant outputs y and control law feedback commands x due to an excitation u. Fast Fourier transform techniques are used to convert time-domain data to the frequency domain, and transfer functions are calculated from the corresponding frequency-domain functions. The controller $\boldsymbol{H}$ and the return-difference matrices and their singular values are then calculated using matrix operations. The computations are described in the following paragraphs. Figure 2 is a flowchart that outlines the CPE procedures.

Transfer Functions

The method used to compute transfer functions is described in Ref. 8. The method therein was extended in the present study to include additional data-windowing capabilities and overlap averaging. Although most control designers used Hanning windows to help smooth data when evaluating their control laws during actual testing, windowing capabilities also include ramp-in/ramp-out, cosine taper, and cosine bell. The overlap-averaging capability allows long time histories to be partitioned into shorter time spans, taking advantage of long periods of time-history data to average out noise, thereby

increasing the statistical quality of the data sample. A zero-fill capability is available to zero fill time history data to an exact block size needed for FFT computations. The overlap-averaging capability with zero fill provided optimum use of the experimental time history data that were obtained.

The controller-output transfer matrix $\boldsymbol{X}_u$ is the matrix of ratios of the cross-spectra of the controller outputs x due to the excitations u to the autospectra of the excitations u; all spectra are obtained from the FFTs of the time histories. Each element of the transfer matrix is given by

$$[\boldsymbol{X}_u(\omega)]_{ij} = \frac{\sum_{m=1}^{N} [S_{u_i x_j}(\omega)]_m}{\sum_{m=1}^{N} [S_{u_i u_i}(\omega)]_m} \tag{1}$$

where N is the number of time history segments. Similarly, each element of the plant-output transfer matrix $\boldsymbol{Y}_u$ is given by Eq. (2):

$$[\boldsymbol{Y}_u(\omega)]_{ij} = \frac{\sum_{m=1}^{N} [S_{u_i y_j}(\omega)]_m}{\sum_{m=1}^{N} [S_{u_i u_i}(\omega)]_m} \tag{2}$$

The two matrices $\boldsymbol{X}_u$ and $\boldsymbol{Y}_u$ are the basis of all subsequent CPE computations. Note that if excitations are added at the command location, Figs. 1a and 1c, the dimensions of $\boldsymbol{X}_{u_c}$ and $\boldsymbol{Y}_{u_c}$ are $n_a \times n_a$ and $n_s \times n_a$, respectively, whereas if the excitations are added at the sensor location, Figs. 1b and 1d, the dimensions of $\boldsymbol{X}_{u_s}$ and $\boldsymbol{Y}_{u_s}$ are $n_a \times n_s$ and $n_s \times n_s$, respectively.

CPE Procedures

For both open- and closed-loop analysis, the return-difference matrices are required. This involves computing $\boldsymbol{HG}$ and $\boldsymbol{GH}$ as well as the plant $\boldsymbol{G}$ and the controller $\boldsymbol{H}$. Table 1, where Eqs. (3a–6d) are given, summarizes the order in which these matrices are computed and the basic equations used in calculating them for both the open- and closed-loop cases in which excitation is added to either the command input to the plant or the sensor input to the controller as depicted in Figs. 1a–1d. To avoid rank-deficient matrices in Eqs. (5), excitations should be added at the command location, Figs. 1a and 1c, corresponding to Eqs. (5a) and (5c), if $n_a > n_s$, and they should be added at the sensor location, Figs. 1b and 1d, corresponding to Eqs. (5b) and (5d), if $n_a < n_s$. Reference 9 provides a more detailed development of the equations for the case in which the excitations are added at the command location.

Open-Loop Case

To perform the first step of the open-loop CPE, the controller transfer matrix $\boldsymbol{H}$, computed using either Eq. (5a) or Eq. (3b), is compared with the designed control law transfer matrix to verify the implementation of the controller. Specifically, the transfer functions are compared for each output/input pair.

To perform the second step in the open-loop CPE (predicting closed-loop performance based on the open-loop performance to decide whether the control law will stabilize or destabilize the system when the loop is closed), it is convenient with a MIMO system to evaluate robustness with respect to multiplicative uncertainties at the plant input and plant output points by examining the corresponding minimum singular values of the return-difference matrices:

$$\underline{\sigma}_{M_I}(\omega) = \sigma_{\min}[(\boldsymbol{I} + \boldsymbol{HG})(\omega)]$$

$$\underline{\sigma}_{M_O}(\omega) = \sigma_{\min}[(\boldsymbol{I} + \boldsymbol{GH})(\omega)] \tag{7}$$

and robustness with respect to an additive uncertainty by examining:

$$\sigma_A(\omega) = \left(\frac{1}{\sigma_{\max}\{[\boldsymbol{H}(\boldsymbol{I} + \boldsymbol{GH})^{-1}](\omega)\}}\right) \tag{8}$$

The matrix product $\boldsymbol{HG}$ is obtained from either Eq. (4a) or Eq. (6b). The matrix product $\boldsymbol{GH}$ can be obtained using Eqs. (6a) or (4b). The singular values of the return-difference matrices can then be determined and observations of the minimum and maximum values over the entire frequency range can be made.

A system crosses the stability boundary at frequencies when $\boldsymbol{I} + \boldsymbol{HG}$ or $\boldsymbol{I} + \boldsymbol{GH}$ is singular and the minimum singular value becomes zero. Therefore the proximity to zero indicates where the system is prone to go unstable and provides a quantitative measure of robustness. Reference 3 contains a derivation that relates guaranteed gain and phase margins to minimum singular values. This relationship is shown in Fig. 3 of the present paper, which is a reproduction of Fig. 2 from Ref. 3 and will be referred to later when discussing results. The ratio of the maximum to minimum singular values of a return-difference matrix is the condition number. If a minimum singular value approaches zero (has low stability margins), the size of the condition number, especially when it is much larger than one, becomes an important indicator of the uncertainty in the measure of system stability; i.e., large condition numbers indicate that the predicted stability margin is very uncertain.

The locus of the determinant of the return-difference matrix as a function of frequency, $\det(\boldsymbol{I} + \boldsymbol{HG})$, has the property that, if the open-loop system is stable, a clockwise encirclement of the critical point (the origin) for $\det[\boldsymbol{I} + \boldsymbol{HG}(\omega)]$ indicates that the controller is destabilizing. Furthermore, the proximity of the determinant locus to the critical point (the origin) is a direct indication of how near the control system

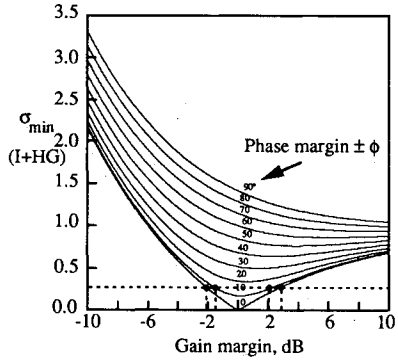

Fig. 3 Universal gain and phase margin diagram.

Table 1 Basic CPE matrix equations[a]

Command excitation		Sensor excitation	
Open loop			
$\boldsymbol{G} = \boldsymbol{Y}_{u_c}$	(3a)	$\boldsymbol{H} = \boldsymbol{X}_{u_s}$	(3b)
$\boldsymbol{HG} = \boldsymbol{X}_{u_c}$	(4a)	$\boldsymbol{GH} = -\boldsymbol{Y}_{u_s}$	(4b)
$\boldsymbol{H} = [(\boldsymbol{Y}_{u_c}\boldsymbol{Y}_{u_c}^T)^{-1}(\boldsymbol{Y}_{u_c}\boldsymbol{X}_{u_c}^T)]^T$	(5a)	$\boldsymbol{G} = -[(\boldsymbol{X}_{u_s}\boldsymbol{X}_{u_s}^T)^{-1}(\boldsymbol{X}_{u_s}\boldsymbol{Y}_{u_s}^T)]^T$	(5b)
$\boldsymbol{GH} = \boldsymbol{G} \cdot \boldsymbol{H}$	(6a)	$\boldsymbol{HG} = \boldsymbol{H} \cdot \boldsymbol{G}$	(6b)
Closed loop			
$\boldsymbol{G} = [(\boldsymbol{I} - \boldsymbol{X}_{u_c}^T)^{-1}\boldsymbol{Y}_{u_c}^T]^T$	(3c)	$\boldsymbol{H} = [(\boldsymbol{I} - \boldsymbol{Y}_{u_s}^T)^{-1}\boldsymbol{X}_{u_s}^T]^T$	(3d)
$\boldsymbol{HG} = [(\boldsymbol{I} - \boldsymbol{X}_{u_c}^T)^{-1}\boldsymbol{X}_{u_c}^T]^T$	(4c)	$\boldsymbol{GH} = -[(\boldsymbol{I} - \boldsymbol{Y}_{u_s}^T)^{-1}\boldsymbol{Y}_{u_s}^T]^T$	(4d)
$\boldsymbol{H} = [(\boldsymbol{Y}_{u_c}\boldsymbol{Y}_{u_c}^T)^{-1}(\boldsymbol{Y}_{u_c}\boldsymbol{X}_{u_c}^T)]^T$	(5c)	$\boldsymbol{G} = -[(\boldsymbol{X}_{u_s}\boldsymbol{X}_{u_s}^T)^{-1}(\boldsymbol{X}_{u_s}\boldsymbol{Y}_{u_s}^T)]^T$	(5d)
$\boldsymbol{GH} = \boldsymbol{G} \cdot \boldsymbol{H}$	(6c)	$\boldsymbol{HG} = \boldsymbol{H} \cdot \boldsymbol{G}$	(6d)

[a]All matrices are functions of ω.

is to an instability. For SISO controllers, this is analogous to the Nyquist plot since in that case

$$\det(\boldsymbol{I} + \boldsymbol{HG}) = \det(\boldsymbol{I} + \boldsymbol{GH}) = 1 + \boldsymbol{GH} \qquad (9)$$

Hence, for an SISO system only, the Nyquist plot is simply a translation of the plot of the determinant of the return-difference matrix about a different critical point $(-1,0)$.

Closed-Loop Case

The difference between closed-loop and open-loop computations is that the transfer matrices $\boldsymbol{X}_u$ and $\boldsymbol{Y}_u$ are obtained experimentally from the closed-loop system. In this case, the open-loop transfer matrices must be extracted from the closed-loop system. The matrix product $\boldsymbol{HG}$ is obtained from either Eq. (4c) or Eq. (6d), and the matrix product $\boldsymbol{GH}$ can be obtained using either Eq. (6c) or Eq. (4d). Singular values can then be determined as for the open-loop case. The singular-value plots are interpreted the same way for closed-loop testing as they were for open-loop testing. Care must be taken, however, in interpreting the determinant plots. If the open-loop plant is unstable with one right-hand pole (for positive frequencies), then the plot will show one counterclockwise encirclement about the origin for a stable closed-loop system. As with the open-loop case, the proximity of the determinant locus to the critical point and the proximity of the minimum singular values to zero are used as measures of closed-loop stability margins.

To obtain results for step 2 of the closed-loop mode, the minimum of the inverse maximum singular value (IMSV)

$$\min_{\omega}\left\{\frac{1}{\sigma_{\max}[\boldsymbol{G}(\omega)]}\right\} \qquad (10)$$

of the open-loop plant transfer matrix, $\boldsymbol{G}$ defined by either Eq. (3c) or Eq. (5d), is an excellent indicator of poles in the proximity of the imaginary axis. The frequency of instability is determined by where the minimum of the IMSV of the plant approaches zero with increasing dynamic pressure. Tracing values of closest approach was a useful way of determining the open-loop plant flutter boundary with respect to some changing test condition, such as dynamic pressure.

Summary of Flutter Suppression Testing

During flutter suppression testing, the control systems were operated in both open-loop and closed-loop modes. For the purpose of maintaining both model and tunnel safety, each candidate control law was initially tested open loop to insure that the control law itself would not destabilize the wind-tunnel model during closed-loop tests. The feedback was digitally switched open at the control law output point, Fig. 1a, and the responses and excitation were collected at the control law input and the control law output locations. The appropriate transfer functions were generated from these responses, and then the CPE capability was exercised to predict the stability of the closed-loop system (Fig. 2). If the control law was predicted to be stable, the switch was closed and the closed-loop flutter suppression (FS) testing for that candidate control law commenced. During the closed-loop testing, the same excitations were inserted and responses were saved as during initial open-loop testing. At each test point, stability margins and open-loop plant stability were determined before proceeding to the next test point.

Description of the CPE Implementation

The digital excitation, actuator commands, and sensor measurements used by the control law were transferred during testing to a SUN 3/160 computer with a SKY Warrior II array processor board where the FFT computations were performed using a FORTRAN 77 program, optimized to take advantage of the vector processing capabilities of the array processor. Each 2K FFT calculation took approximately 0.003 s. The matrix computations to obtain the singular values of return-difference matrices were also performed on the SUN 3/160 using MATLAB software operations.[10] Figure 2 outlines the separate codes.

Results and Discussion

Both SISO and MIMO flutter suppression control laws were designed for the AFW wind-tunnel model. During the wind-tunnel test, four FS control laws were tested using the AFW digital controller.[7] Experimental data were used to evaluate their performance using the CPE capability presented in this paper. The process of obtaining experimental data and evaluating performance is described in the following.

The data for performing CPE were obtained by exciting, one at a time, all pairs of control surfaces used by the control law. Results from two tests performed in 1989 and in 1991 are presented in this paper. The excitation usually used in the 1989 tests was a 150 s logarithmic sine sweep (LogSS) over a frequency range varying from 4 to 35 Hz. However, low amplitude excitations, having low signal-to-noise ratios, were required at high dynamic pressures to keep the excitation itself from inducing flutter. The resulting CPE was poor and sometimes inconclusive. In the 1991 tests, a periodic pseudonoise (PPN) over a frequency range varying from 3 to 20 Hz was generally used. The PPN (described in the Appendix) was designed to maximize the amplitude of the excitation (allowing maximum signal-to-noise ratio) within the actuator rate limits for a prescribed frequency range and specified frequency resolution. Typical transfer functions at one test condition resulting from both a logarithmic sine sweep and a PPN excitation are shown in Fig. 4. These results demonstrate that the PPN excitation, over the frequency range for which it was designed, provides smoother and more reliable results than the LogSS excitation.

When FS control laws were required to control symmetric and/or antisymmetric flutter, the CPE excitation was added to the control surfaces either symmetrically or antisymmetrically, depending on which symmetry was being evaluated. The responses y were then summed or differenced, depending on symmetry, before saving. While stability computations were being performed for symmetric control, the antisymmetric excitations could be performed and the transfer matrices generated. Final results and plots were available within 2 min after the last excitation was performed.

Figure 5 shows an h line (dynamic pressure vs Mach number) plot with three test points identified that correspond to the points at which test results are presented herein. Points A and B correspond to cases for which an SISO control law is operating closed loop and the plant is stable (A) and unstable (B). Point C identifies a test point at which another control law (in this case a MIMO) would destabilize a stable plant if the loop were closed. CPE results are presented in the following discussions.

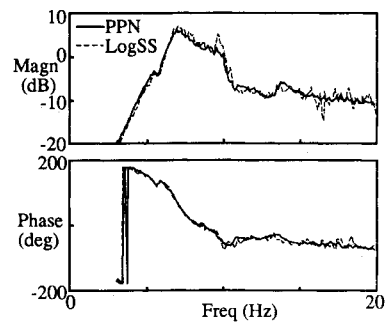

Fig. 4 Comparison of transfer function $\ddot{z}_{TIP}/\delta_{TEO}$ for periodic random noise and logarithmic sine sweep excitation.

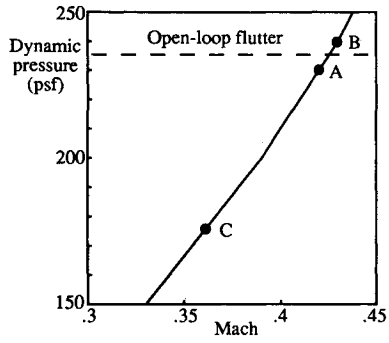

Fig. 5 Atmospheric h line showing flutter boundary and points for which results will be presented.

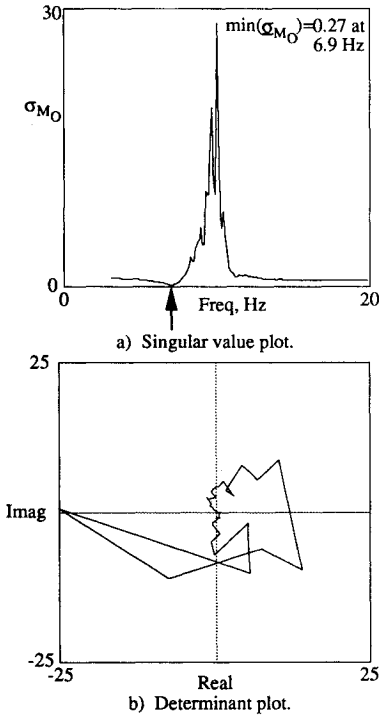

Fig. 6 Closed-loop CPE results for a symmetric SISO control law (open-loop plant is stable), $M = 0.42$, $q = 230$ psf.

SISO Control Law

Typical CPE results for a symmetric SISO control law obtained during the closed-loop wind-tunnel tests are shown in Figs. 6 and 7. The determinant plot in Fig. 6 shows no encirclement about the origin (the critical point) at a dynamic pressure of 200 psf where the open-loop plant is known to be stable (point A of Fig. 5). Figure 7 shows the CPE results of a closed-loop system where the plant is unstable (point B on Fig. 5). Since there is one net encirclement of the critical point, these plots indicate that the controller is stabilizing the plant. Using the minimum singular value from Fig. 7, guaranteed stability margins can be obtained from the universal gain and phase diagram of Fig. 3. Since the minimum of $\underline{\sigma}_{M_O}$ is 0.29, the gain margin for zero phase margins are approximately -2.2 and $+2.7$ db, and for a 10-deg phase margin, the gain margins are -1.4 and $+2.1$ db.

MIMO Control Law

Results for an MIMO FS control law design (Ref. 6 with increased gain) are presented next. The initial open-loop testing performed at 150 psf indicated that the controller would not destabilize the model; hence the loop was closed and testing continued. At approximately 175 psf, the closed-loop system appeared to become unstable where the open-loop plant was known to be stable. Consequently, open-loop testing was performed at 175 psf. The plots of $\underline{\sigma}_{M_I}$ and $\underline{\sigma}_{M_O}$ for the MIMO system are shown in Fig. 8 along with the maximum singular values $\overline{\sigma}_{M_I}$ and $\overline{\sigma}_{M_O}$ to provide a visual indication of the condition number. Figure 8 also contains the singular values for the evaluation of the additive perturbation σ_A. The locus of the determinants of $\boldsymbol{I} + \boldsymbol{HG}$ (lower right) shows an encirclement of the origin where the open-loop plant is known to be stable, thus indicating that the MIMO control law would be destabilizing as indicated during previous closed-loop testing. As discussed previously, large condition numbers indicate uncertainty in the computation of the minimum singular values. Referring to the upper plot of Fig. 8, the ratio of the maximum $\overline{\sigma}_{M_O}$ to the minimum singular value $\underline{\sigma}_{M_O}$ (i.e., condition number) is large only in the vicinity of 7 Hz. Therefore, the low stability margins indicated by the minimum singular values in the vicinity of 20 Hz are fairly certain. Upon further

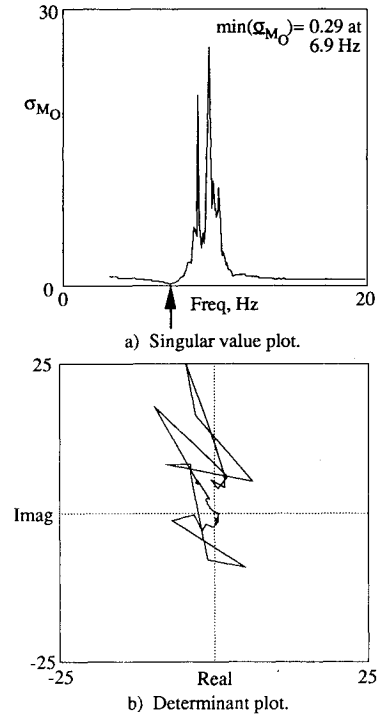

Fig. 7 Closed-loop CPE results for a symmetric SISO control law (open-loop plant is unstable), $M = 0.43$, $q = 240$ psf.

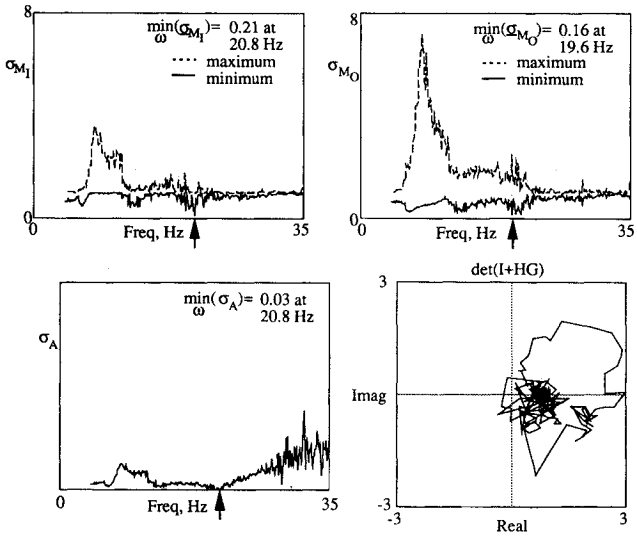

Fig. 8 Open-loop CPE results for a symmetric MIMO control law (open-loop plant is stable), $M = 0.36$, $q = 175$ psf.

investigation, one of the elements of this destabilizing controller transfer matrix was examined and plots of the transfer function showed a peak magnitude close to 20 Hz.

Flutter Prediction

One of the objectives of the wind-tunnel testing was to determine the open-loop flutter dynamic pressure from closed-loop experimental data. A method of determining whether the open-loop plant is stable or unstable is to count encirclements of the critical point in the determinant plot, as described in a previous section of the paper. Figure 6 shows no net encirclement of the critical point. Since the closed-loop system is stable, this indicates the open-loop plant is stable. Figure 7 shows one counterclockwise encirclement of the critical point, indicating the open-loop plant is unstable with one unstable pole (for positive frequencies). Figures 6 and 7 established that the flutter boundary was between 230 and 240 psf for the single-input/single-output control system. Even though this prediction does not give a definite quantitative measure of the flutter boundary, it does set limits on where open-loop flutter occurs by setting upper and lower boundaries of where the open-loop system reaches neutral stability.

A more quantitative definition of the open-loop flutter boundary is obtained by tracking the minimums of the inverse maximum singular values (IMSV) [Eq. (10)] of the plant extracted from closed-loop experimental data as a function of dynamic pressure. To do this, the IMSV are plotted as a function of frequency at each dynamic pressure. An example for a dynamic pressure of 150 psf is given in Fig. 9. The global minimum of the curve, identified by the arrow, indicates the mode that is going unstable and its frequency. The magnitude of this point approaching zero indicates the proximity of the flutter mode of the open-loop system to neutral stability. Curves with two minimums approaching zero would indicate flutter is probably a result of two modes coalescing. In this case, the frequencies of the two modes coalesce at flutter.

A plot of the minimums from figures such as Fig. 9 are then plotted as a function of dynamic pressure. In this example, shown in Fig. 10, only one "global" minimum is being traced. Since the number of data points was limited, the dashed part of the curve indicates the "best estimate" of the trajectory toward an instability. The point at which the inverse maximum singular values is zero is the point at which open-loop flutter occurs. This point, approximately 232 psf, is the predicted flutter dynamic pressure. Later open-loop testing to determine the actual open-loop flutter boundary indicated that the actual symmetric boundary point was 235 psf. This value corresponds well with the flutter prediction using plant transfer matrices extracted from closed-loop experimental data.

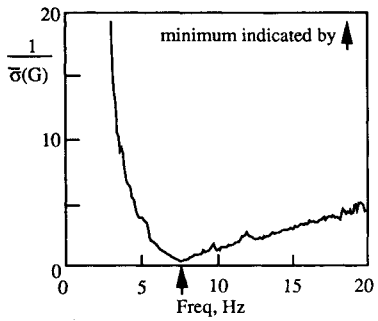

Fig. 9 Plot of inverse maximum singular values of the open-loop plant transfer matrix, q = 150 psf.

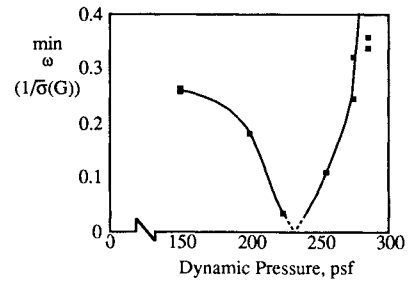

Fig. 10 Flutter prediction using closed-loop CPE results.

Conclusions

A controller performance evaluation (CPE) methodology was developed to evaluate the performance of multivariable, digital control systems. The method was used and subsequently validated during the wind-tunnel testing of an aeroelastic model equipped with a digital flutter suppression controller. Through the CPE effort, a wide range of sophisticated real-time analysis tools were developed. These tools proved extremely useful and worked very well during wind-tunnel testing. Moreover, results from open-loop CPE were the sole criteria for beginning closed-loop testing. In this way, CPE identified potentially destabilizing controllers before actually closing the loop on the control system, thereby helping to avoid catastrophic damage to the wind-tunnel model or the tunnel. CPE results also proved useful in determining open-loop plant stability during closed-loop test conditions.

Appendix

The periodic pseudonoise (PPN) excitation developed for use in the AFW wind-tunnel test was developed to have a specific frequency content and to allow for maximum excitation amplitude subject to constraints on the rate. It is similar to periodic random noise or pseudorandom noise described in Ref. 11, but it is not truly random and has a specified frequency content. It is generated by picking a block size that determines the frequency resolution. Time histories of sine waves with these frequencies over a finite time range defined by the block size are added or subtracted. Whether they are added or subtracted depends on which causes the least amount of increase in the maximum rate. After all of the time histories have been added, the excitation is divided by the maximum amplitude to obtain an excitation with a unity maximum amplitude. The time histories are added together starting with the sine sweep of the highest frequency.

Acknowledgments

The authors wish to thank William M. Adams, Jr., for his continued insistence on the need for an on-line real-time controller performance evaluation capability and to acknowledge his original outline for the CPE procedures and the development of the periodic pseudonoise excitation described herein. Any questions with regard to this PPN should be addressed to William Adams. We would also like to thank Boyd Perry, III, for his coordination and guidance in carrying through the CPE effort.

References

[1]Mukhopadhyay, V., and Newsom, J. R., "A Multiloop System Stability Margin Study Using Matrix Singular Values," *Journal of Guidance, Control, and Dynamics*, Vol. 7, No. 5, 1984, pp. 582–587.

[2]Mukhopadhyay, V., and Newsom, J. R., "Application of Matrix Singular Value Properties for Evaluating Gain and Phase Margins of Multiloop Systems," AIAA Paper 82-1574, Aug. 1982.

[3]Mukhopadhyay, V., Pototzky, A. S., and Fox, M. E., "A Scheme for Theoretical and Experimental Evaluation of Multivariable System Stability Robustness," *Proceedings of the 1990 American Control Conference*, American Automatic Control Council, Green Valley, AZ, 1990, pp. 3046–3047; also, Paper FP 14-5, May 1990.

[4]Miller, G. D., "Active Flexible Wing (AFW) Technology," Air Force Wright Aeronautical Labs., AFWAL TR-87-3096, Wright-Patterson AFB, OH, Feb. 1988.

[5]Noll, T., Perry, B., III, Hoadley, S. T., Cole, S. R., Buttrill, C. S.,

Adams, W. M., Jr., Houck, J. A., Srinathkumar, S., Mukhopadhyay, V., Pototzky, A. S., Heeg, J., McGraw, S. M., Miller, G., Ryan, R., Brosnan, M., Haverty, J., and Klepl, M., "Aeroservoelastic Wind Tunnel Investigations Using Active Flexible Wing Model—Status and Recent Accomplishments," AIAA Paper 89-1168, April 1989; also, NASA TM-101570, April 1989.

[6]Perry, B., III, Mukhopadhyay, V., Hoadley, S. T., Cole, S. R., Buttrill, C. S., and Houck, J. A., "Digital-Flutter-Suppression-System Investigations for the Active Flexible Wing Wind-Tunnel Model," AIAA Paper 90-1074, April 1990; also, NASA TM-102618, March 1990.

[7]Hoadley, S. T. and McGraw, S. M., "The Multiple-Function Multi-Input/Multi-Output Digital Controller System for the AFW Wind-Tunnel Model," *Proceedings of the AIAA Dynamic Specialist Conference*, AIAA, Washington, DC, 1992, pp. 30–38; also, NASA TM-107600, May 1992.

[8]Adams, W. M., Jr., Hoadley, S. T., and Bardusch, R. E., "Active Suppression of an 'Apparent Shock Induced Instability,'" *Proceedings of the AIAA 28th Structures, Structural Dynamics, and Materials Conference*, AIAA, Washington, DC, 1987, pp. 491–498; also, AIAA Paper 87-0881, April 1987.

[9]Pototzky, A. S., Wieseman, C. D., Hoadley, S. T., and Mukhopadhyay, V., "Development and Testing of Methodology for Evaluating the Performance of Multi-Input/Multi-Output Digital Control Systems," *Proceedings of the AIAA Guidance, Navigation, and Control Conference*, AIAA, Washington, DC, 1990, pp. 1673–1682, also, AIAA Paper 90-3501, Aug. 1990; also NASA TM-102704, Aug. 1990.

[10]*PRO-MATLAB User's Guide*, Math Works, Inc., South Natick, MA.

[11]Olsen, N., "Excitation Functions for Structural Frequency Response Measurements," 2nd International Modal Analysis Conference, Orlando, FL, 1984, pp. 894–902.